

JAMES | Journal of Advances in Modeling Earth Systems*



RESEARCH ARTICLE

10.1029/2022MS003035

Key Points:

- The complex topography over the Tibetan Plateau greatly influences the snow cover distribution in winter
- Using the snow cover fraction (SCF) schemes without topography leads to a consistent positive bias of SCF simulations in winter
- By adding a topographic factor, the simulations of winter SCF and surface albedo are significantly improved

Correspondence to:

W. Guo, guowd@nju.edu.cn

Citation:

Miao, X., Guo, W., Qiu, B., Lu, S., Zhang, Y., Xue, Y., & Sun, S. (2022). Accounting for topographic effects on snow cover fraction and surface albedo simulations over the Tibetan Plateau in winter. *Journal of Advances in Modeling Earth Systems*, 14, e2022MS003035. https://doi.org/10.1029/2022MS003035

Received 9 FEB 2022 Accepted 16 AUG 2022

Author Contributions:

Conceptualization: Xin Miao, Weidong Guo Data curation: Xin Miao Formal analysis: Xin Miao Investigation: Xin Miao Methodology: Xin Miao, Weidong Guo,

Bo Qiu

Software: Xin Miao, Sha Lu Supervision: Weidong Guo, Yu Zhang, Yongkang Xue, Shufen Sun Validation: Xin Miao Visualization: Xin Miao Writing – original draft: Xin Miao

Writing – review & editing: Weidong Guo, Bo Qiu, Yu Zhang, Yongkang Xue, Shufen Sun

© 2022 The Authors. Journal of Advances in Modeling Earth Systems published by Wiley Periodicals LLC on behalf of American Geophysical Union. This is an open access article under the terms of the Creative Commons Attribution-NonCommercial License, which permits use, distribution and reproduction in any medium, provided the original work is properly cited and is not used for commercial purposes.

Accounting for Topographic Effects on Snow Cover Fraction and Surface Albedo Simulations Over the Tibetan Plateau in Winter

Xin Miao¹, Weidong Guo¹, Bo Qiu¹, Sha Lu¹, Yu Zhang², Yongkang Xue³, and Shufen Sun⁴

¹School of Atmospheric Sciences, Nanjing University, Nanjing, China, ²Plateau Atmosphere and Environment Key Laboratory of Sichuan Province, School of Atmospheric Sciences, Chengdu University of Information Technology, Chengdu, China, ³Department of Geography and Department of Atmospheric and Oceanic Sciences, University of California, Los Angeles, Los Angeles, CA, USA, ⁴State Key Laboratory of Numerical Modeling for Atmospheric Sciences and Geophysical Fluid Dynamics, Institute of Atmospheric Physics, Chinese Academy of Sciences, Beijing, China

Abstract The Tibetan Plateau (TP) is the highest land in the world and has a very complex topography. However, the influence of topography on TP snow cover simulations has not been adequately addressed in most land surface models. The analysis of satellite observations indicates that snow cover fraction (SCF) simulation biases increase with the topography complexity, and this increasing trend slows down when the standard deviation of topography is greater than 200 m. The result also shows that using the SCF schemes without consideration of topography leads to a consistent overestimation in winter. To account for the topographic effects, we introduce a modified topographic factor to the SCF schemes. Then we conduct regional simulations using the Simplified Simple Biosphere Model version 3 (SSiB3) and evaluate the results at the location of observation sites to reduce the uncertainty induced by forcing data. Compared with the default SCF scheme, the mean winter SCF bias is reduced from 3.83% to -0.10%. The optimization of SCF simulations further improves the winter surface albedo and land surface temperature (LST) simulations. The winter surface albedo bias over the TP is reduced from 0.020 to 0.007, with a maximum reduction by -0.133. The winter LST bias is reduced from -3.33 to -3.04 K, with a maximum reduction by 3.60 K. This study highlights the importance of topographic effects in simulating snow cover distribution and land surface energy budget for reducing the "cold bias" in winter climate simulations over the TP.

Plain Language Summary The Tibetan Plateau (TP) has a very complex topography, which greatly influences the snow cover distribution in winter. However, the influence of topography on snow cover simulations has not been adequately addressed in most land surface models. Based on the satellite data, we find that ignoring topography leads to a significant overestimation of the simulated snow cover distribution over the TP in winter, and the overestimation increases with the topographic complexity until the terrain complexity reaches a certain level. By applying this relationship, the winter snow cover distribution simulations are greatly improved over the TP, and this improvement further leads to the improvement of land surface energy budget simulations in winter. Taking the topographic effect on snow cover distribution into account contributes to reducing the "cold bias" in winter climate simulations over the TP.

1. Introduction

The Tibetan Plateau (TP), which is also known as "The Third Pole," is the highest land area in the world and has widespread seasonal snow cover. In the past 50 years, the TP has undergone dramatic changes characterized by imbalances in the warming climate, such as accelerated glacier retreats, permafrost degradation, lake expansions, and snow cover change (S. Kang et al., 2010; Yao, Wu, et al., 2019; Yao, Xue, et al., 2019). The interannual trends in snow cover over the TP for the last 40–50 years show remarkable regional and seasonal differences (You et al., 2020). The use of different data set. also affects the evaluation of trends in TP snow cover (Bian et al., 2020; You et al., 2020). In addition to the interannual variation, the strong solar radiation, high elevations, and complex terrains over the TP also lead to high spatial and temporal variabilities in the snow cover distribution. The variability of different time scales in seasonal snow cover over the TP influences the land-atmosphere energy exchange process, thereby influencing the weather and climate of the TP and its surrounding areas (H. Zhao & Moore, 2004; Li et al., 2018; P. Zhao et al., 2007; Seol & Hong, 2009; Wu & Qian, 2003; Xiao et al., 2016).

MIAO ET AL. 1 of 18



On the TP, in-situ observations are very limited due to the harsh environment. Therefore, numerical simulations are necessary for snow cover and climate research. However, a common "cold bias" exists in the near-surface temperature simulations in current global climate models and regional climate models (Cui et al., 2021; Meng et al., 2018; Su et al., 2013; Y. Gao et al., 2015). This "cold bias" may be attributed to precipitation ice radiative effects (Lee et al., 2019), "wet bias" (Duan et al., 2013), overestimated snow cover (Lalande et al., 2021; X. Chen et al., 2017), aerosols in the snow (Usha et al., 2020) and other causes. Meng et al. (2018) reduced the "cold bias" of simulated near-surface air temperature over the TP by updating the surface albedo based on the Moderate Resolution Imaging Spectroradiometer (MODIS) product and indicated that the "cold bias" is probably caused by the bad simulations of snow cover. During the snow season, especially in winter, the change in surface albedo over the TP is dominated by the variation in snow cover. W. Wang, Yang, et al. (2020) proposed a new albedo scheme for shallow fresh snow over the TP, and the snow simulation bias was greatly reduced. In addition to the snow albedo, the overestimation of snow cover areas may also lead to the overestimation of surface albedo, and thus cause the "cold bias" in the near-surface air temperature simulations.

In climate models and land surface models, snow cover fraction (SCF) parameterizations are widely used to calculate the snow cover area percentages of model grids. Dickinson et al. (1993) developed a SCF parameterization scheme in the Biosphere-Atmosphere Transfer Scheme, which depends on the snow depth (SDP) and ground roughness (Z_{0p}) . After that, different SCF schemes were developed in several studies (Bonan, 1996; Marshall & Oglesby, 1994; Marshall et al., 1994; Niu & Yang, 2007; Sellers et al., 1996; Sun & Xue, 2001; Wu & Wu, 2004; Z. L. Yang et al., 1997), but none of these parameterization schemes accounted for the influence of topography on the SCF simulations. Douville et al. (1995) used snow water equivalent (SWE) to calculate SCF and introduced topographic factors to consider the influence of topography on SCF in mountainous areas, and used the standard deviation of topography (SDtopo) to represent the topographic complexity. Based on this, Roesch et al. (2001) developed a new scheme considering both hyperbolic functions and the influence of topography on SCF. After that, Swenson and Lawrence (2012) developed a new SCF scheme for the Community Land Model (CLM) based on daily satellite observations to consider both the influence of topography and the differences between the snow accumulation period and snowmelt period. This new scheme also used SDtopo to represent the topographic complexity. In addition, in the recently released land surface model Beijing Climate Center Atmosphere-Vegetation Interaction Model version 2.0, Li et al. (2019) modified the SCF scheme by combining the schemes of Yang et al. (1997) and Roesch et al. (2001).

In recent years, several researchers have evaluated the simulation effects of different SCF schemes in land surface modeling on the TP. Xie et al. (2018) evaluated the simulation differences of two SCF schemes on the TP using the CLM 4.5 based on the Interactive Multisensor Snow and Ice Mapping System snow cover products and pointed out that the scheme from Niu and Yang (2007) overestimated the SCF on the TP, while the scheme from Swenson and Lawrence (2012) underestimated it. Based on the MODIS and FY-3B snow cover products, Jiang et al. (2020) optimized the SCF schemes in Noah-MP and reduced the overall bias of SCF simulation. The TP is the highest and youngest natural geographical unit in the world. The rapid uplift and unroofing of southern Tibet began approximately 20 million years ago, and the present elevation of much of the TP was attained approximately 8 million years ago (Harrison et al., 1992). The TP and its surrounding areas also have a very complex topography (shown in Figure 1). The edge of the TP has large fluctuations, while the interior of the TP is flat. Due to the complex topography and strong radiation on the TP, the characteristics of snow cover on the TP are quite different from those in high-latitude areas (J. Wang et al., 2018; Qin et al., 2006), indicating that the snow parameterization schemes must be evaluated and modified with the consideration of complex topography over the TP. However, the influence of topography on SCF simulations on the TP has not been evaluated in previous studies. Accurately optimizing the bias in SCF simulations caused by the topography on the TP also remains challenging.

In this study, we analyze the influence of topography on SCF simulations based on satellite observations, evaluate the simulation effects of six SCF schemes in the Simplified Simple Biosphere Model version 3 (SSiB3) land surface model and try to reduce the SCF simulation bias that arises due to topography by introducing a topographic factor to the original schemes. Section 2 describes the details of the data used in this study, the SSiB3 land surface model, the topographic factors, and the experimental design. The simulation results are presented in Section 3. The discussion and conclusions are presented in Sections 4 and 5, respectively.

MIAO ET AL. 2 of 18



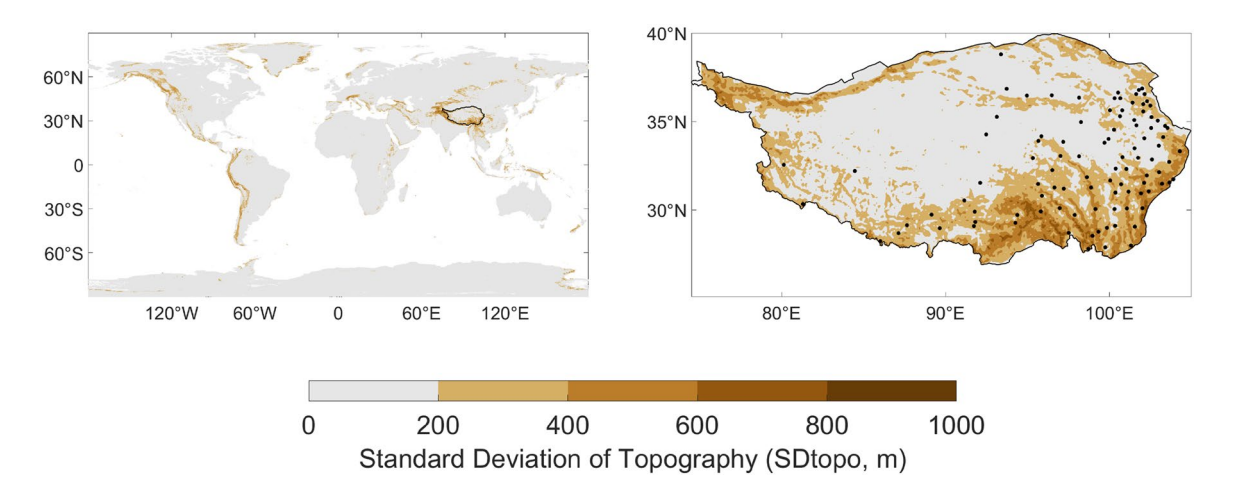


Figure 1. Global 0.1° standard deviation of topography (SDtopo, unit: m) (left) and that of the Tibetan Plateau (TP; right); location of 99 China Meteorological Administration stations over the TP (right).

2. Data and Method

2.1. Meteorological Forcing Data and Input Data

The SSiB3 model is driven by the China Meteorological Forcing Dataset (CMFD; http://data.tpdc.ac.cn/en/data/8028b944-daaa-4511-8769-965612652c49/; He et al., 2020; K. Yang et al., 2010). The CMFD is one of the state-of-the-art near-surface meteorological data sets with a gridded spatiotemporal resolution that was developed specifically for studies of land surface processes in China. The data set was made through the fusion of remote sensing products, reanalysis data sets, and in-situ observation data recorded at weather stations (He et al., 2020). The data set, with a temporal resolution of 3 hr from 1979 to 2018 and a spatial resolution of 0.1°, includes 2-m air temperature, surface pressure, specific humidity, 10-m wind speed, downward shortwave radiation, downward longwave radiation, and precipitation rate values.

The leaf area index (LAI) in the original SSiB3 model is obtained using a look-up table for different land cover types and months. We use 0.1°, multiyear mean (2000–2015) LAI data obtained from the Land-Atmosphere Interaction Research Group at the Sun Yat-sen University (http://globalchange.bnu.edu.cn/research; Yuan et al., 2011) to replace the default LAI parameter values. The 2015 Terra and Aqua Combined MODIS Land Cover Yearly L3 Global 0.05° Climate Modeling Grid (MCD12C1) product (https://doi.org/10.5067/MODIS/MCD12C1.006) is used to replace the original land cover map in SSiB3.

A 0.008° elevation data set for the TP (available at http://data.tpdc.ac.cn/en/data/ddf4108a-d940-47ad-b25c-03666275c83a/) is input to calculate the gridded SDtopo. The elevation data set is made based on NASA Digital Elevation Model (DEM) elevation data integrating terrain slope and referencing mountain integrity and ecosystem integrity. The 0.1° SDtopo data are obtained by calculating the standard deviation of all DEM data in the 0.1° grid cell.

2.2. Validation Data

The daily cloudless MODIS snow area ratio data set of the TP (https://data.tpdc.ac.cn/en/data/94a8858b-3ace-488d-9233-75c021a964f0/; Tang et al., 2013) is used to validate the simulated SCF in this study. The daily cloudless MODIS snow area ratio data set (2000–2015) of the TP is obtained by using a cloud removal algorithm based on cubic spline interpolation to optimize the MODIS daily snow product MOD10A1. The data set is projected by Universal Transverse Mercator Grid System with a spatial resolution of 500 m, providing daily SCF results in the TP. We average the original data with a spatial resolution of 500 m based on the coordinate to derive 0.1° SCF data in this study.

We use a daily, 0.05° SDP data set for the TP (https://data.tpdc.ac.cn/en/data/0515ce19-5a69-4f86-822b-330aa11e2a28/; Yan et al., 2021) in this study. The SDP data set is derived from the fusion of the snow cover probability data set and the long-term SDP data set in China. A subpixel downscaling algorithm is developed to

MIAO ET AL. 3 of 18

Table 1			
Snow Cover Fraction (SCF)	Schemes Use	ed in the	Simulations

CTL			ТОРО
MO94	$f \operatorname{sno} = \frac{\operatorname{SDP}}{\operatorname{SDP} + Z_{0g}}$	MO94T	$f \operatorname{sno} = \frac{\operatorname{SDP}}{\operatorname{SDP} + Z_{0g}} \cdot \left(\frac{\operatorname{SDP}}{\operatorname{SDP} + \epsilon + 0.0002 \cdot \sigma}\right)^{a}$
BO96	$f \operatorname{sno} = \min\left(\frac{\operatorname{SDP}}{0.05}, 1\right)$	BO96T	$f \operatorname{sno} = \min\left(1, \frac{\operatorname{SDP}}{0.05} \cdot \left(\frac{\operatorname{SDP}}{\operatorname{SDP} + \epsilon + 0.0002 \cdot \sigma}\right)^{a}\right)$
SX01	$f sno = \min\left(\frac{swe}{0.004}, 1\right)$	SX01T	$f \operatorname{sno} = \min\left(1, \frac{\operatorname{SWE}}{0.004} \cdot \left(\frac{\operatorname{SDP}}{\operatorname{SDP} + \varepsilon + 0.0002 \cdot \sigma}\right)^{a}\right)$
NY07	f sno = tan $h\left(\frac{\text{SDP}}{2.5Z_{0g}\left(\rho_{\text{sno}}/\rho_{\text{new}}\right)^m}\right)$	NY07T	$f \operatorname{sno} = \tanh \left(\frac{\operatorname{SDP}}{2.5 Z_{0g} \left(\rho_{\operatorname{Sno}} / \rho_{\operatorname{new}} \right)^m} \right) \cdot \left(\frac{\operatorname{SDP}}{\operatorname{SDP} + \varepsilon + 0.0002 \cdot \sigma} \right)^a$
SL12	In the SL12T scheme, set $\sigma = 10$ (Flat Topography)	SL12T	$f_{\rm sno}^{\rm snowfall} = 1 - ((1 - \tanh(k_{\rm accum}q_{\rm sno}\Delta t))(1 - f_{\rm sno}^n)$
			$f_{\text{sno}}^{\text{snowmelt}} = 1 - \left(\frac{1}{\pi}\cos^{-1}\left(2\frac{\text{SWE}}{\text{SWE}_{\text{max}}} - 1\right)\right)^{N_{melt}}, \text{Nmelt} = \frac{200}{\max(10.\sigma)}$
LI19	$f \operatorname{sno} = \tanh\left(\frac{\operatorname{SDP}}{2.5Z_{0g}}\right)$	LI19T	f sno = tan $h\left(\frac{\text{SDP}}{2.5Z_{0g}}\right) \cdot \left(\frac{\text{SDP}}{\text{SDP} + \epsilon + 0.0002 \cdot \sigma}\right)^{a}$

Note. Z_{0g} is the ground roughness ($Z_{0g} = 0.01 \text{ m}$), ρ_{new} is the new snow density ($\rho_{new} = 100 \text{ kg/m}^3$), m is the melting factor (m = 1.0, the default value in Noah-MP), k_{accum} is the snow accumulation coefficient ($k_{accum} = 0.1$), $q_{sno}\Delta t$ is the amount of new snow that falls within Δt , σ is the standard deviation of topography within the 0.1° grid, a is an adjustable constant smaller than 1 according to the spatial resolution of the model grid cell and a is set to 0.5 in this study following Roesch et al. (2001), and ε is set as a small number to avoid dividing by 0. Notably, snow cover fraction (SCF), snow water equivalent (SWE), and SWE_{max} are updated after the snow accumulation event in SL12.

downscale the original 0.25° SDP data set, and derive the 0.05° daily SDP product. For the 92 meteorological stations of the China Meteorological Administration (CMA) over the TP, the average root mean square error (RMSE) value is reduced from 2.15 to 1.54 cm, and the average mean absolute error (MAE) is reduced from 1.12 to 0.67 cm.

We also use albedo data from the Global Land Surface Satellite (GLASS) product (http://www.glass.umd.edu; Liang, Zhang, et al., 2013; Liang, Zhao, et al., 2013, 2020) to evaluate the surface albedo simulation results obtained in this study. We generate monthly surface albedo data from the 8-day clear-sky shortwave albedo data according to the method outlined in F. Gao et al. (2014). Previous studies have evaluated the accuracy of GLASS albedo products (A. Chen et al., 2015, 2020; L. Wang et al., 2014). A. Chen et al. (2015) indicated that GLASS albedo data probably overestimates the surface albedo due to the influence of clouds, and GLASS albedo is lower than in-situ observation due to snow cover. Compared to MODIS albedo data, GLASS albedo data shows a better spatial continuity and inversion quality. Furthermore, MODIS and GLASS albedo data can both match the in-situ observations based on the TP, and GLASS performs better during the snow period (Chen et al., 2020).

The MODIS daily land surface temperature (LST) product (https://modis.gsfc.nasa.gov/data/dataprod/mod11. php; Wan, 2014) is used to validate the LST simulations in this study. The MODIS LST product has good spatiotemporal continuity, which makes up for the lack of sparse observational data on the TP. The data have been widely used to investigate the LST variations over the TP (M. Yang et al., 2021; Ouyang et al., 2012; Xu et al., 2013). The data are also preprocessed by monthly synthetic cloud removal processing (taking the cloud-free phase surface temperature values in each month for average processing and obtaining the monthly average daytime and nighttime surface temperatures) before validation.

2.3. Land Surface Model Simplified Simple Biosphere Model Version 3

The SSiB land surface model was developed by Xue et al. (1991) and has evolved with several versions. SSiB version 3 (SSiB3; Sun & Xue, 2001) is coupled with the Snow-Atmosphere-Soil Transfer (SAST) snow model (Sun et al., 1999; Zhong, Li, Sun, Chen, & Wen, 2017; Zhong, Li, et al., 2017). SAST presents a snow cover model and originally deals with the atmosphere-snow-soil continuum only. There is no direct interaction between vegetation and snow cover in the original SAST.

In SSiB3, there are 13 land cover types, and snow-vegetation interactions are taken into consideration. The effects of vegetation on snow radiation and hydrological processes are considered separately based on different vegetation types. The snowpack in SSiB3 is one layer of thin snow or divided into three layers if the SDP is larger than 7 cm. The SCF is determined by the SWE (see Table 1). In SSiB3, the surface albedo is calculated based

MIAO ET AL. 4 of 18



on canopy and ground albedos, weighted by vegetation cover fraction. The canopy albedo calculation considers the snow-on-vegetation effect, while the ground albedo is calculated by the soil and snow albedos, weighted by the SCF. Based on the overall surface albedo, the SSiB3 model calculates the overall surface energy balance processes for all areas (snow and non-snow areas). However, the snow albedo parameterization in SSiB3 is empirical, and the snow radius change and aerosol deposition have not been taken into account.

2.4. Standard Deviation of Topography and Topographic Factor

Compared to the average topographic height, the SDtopo metric better represents the variations in topography that cause irregular snow cover distributions in mountainous areas (Douville et al., 1995). In previous studies, SDtopo has been widely used to describe the variabilities in topography (Douville et al., 1995; Li et al., 2019; Roesch et al., 2001; Swenson & Lawrence, 2012). SDtopo is also used in this paper as an index to represent the topography complexity, and the 0.1° SDtopo data are obtained by calculating the standard deviation of all DEM data in a 0.1° grid cell.

In SCF simulations, the influence of topography is related to the topographic complexity and snow amount. The more complex the terrain is, the more uneven the distribution of snow cover, resulting in a smaller snow extent for the same amount of snow. For the same state of topography, more snow accumulation will reduce the impact of topography. To reduce the SCF simulation bias caused by topography, Douville et al. (1995) first proposed a topographic factor ($\sqrt{\frac{1,000SWE}{1,000SWE+0.15\sigma}}$), a function of SDtopo, to calculate the topographic effect in SCF simulations ($f_{sno}(SDP, \sigma) = f_{sno}(SDP) \times Topographic Factor$, where f_{sno} is the SCF and σ is the SDtopo). Roesch et al. (2001) continued to use this topographic factor to reduce the SCF simulation bias with a slight modification ($\sqrt{\frac{1,000SWE}{1,000SWE+\varepsilon+0.15\sigma}}$). Li et al. (2019) further modified the topographic factor ($\sqrt{\frac{SDP}{SDP+\varepsilon+0.0002-\sigma}}$) on the basis of Roesch et al. (2001). For example, in the scheme of Li et al. (2019), SDtopo (σ) and the SDP represent the topographic complexity and the amount of snow, respectively. The larger the SDtopo or the smaller the SDP is, the smaller the topography factor, and the greater the influence of topography on the SCF simulation. Over the TP, the influence of topography is more obvious due to thin snow and complex topography (Figures 1, 3a and 3b). This suggests that the influence of topography on SCF simulations over the TP is nonnegligible.

2.5. Experimental Design

To investigate the influence of different SCF schemes in the TP snow cover simulations, we select six SCF schemes in different land surface models/snow models, namely, MO94 (Marshall & Oglesby, 1994), BO96 (Bonan, 1996), SX01 (Sun & Xue, 2001; here, we use the formula in SSiB3), NY07 (Niu & Yang, 2007), SL12T (Swenson & Lawrence, 2012; here, we use the formula in CLM 5.0) and LI19T (Li et al., 2019). A "T" in a scheme name indicates that the scheme includes the topographic effect. Among the six SCF schemes, the MO94, BO96, SX01, and NY07 functions are all based on the empirical relationship of SCF and SDP/SWE without considering topography. To compare the six schemes without topography, we set the SDtopo value in the SL12T scheme to the minimum value for all areas and derived the SL12 scheme. We also remove the topographic factor in the LI19T scheme and derive the LI19 scheme, which is the same as the scheme of Yang et al. (1997).

To investigate the influence of topography on SCF simulations, we first calculate the winter (December, January, and February) SCF based on the 0.1° SDP data and five SCF schemes without topography (MO94, BO96, SX01, NY07, and LI19; SL12 is excluded because it is calculated based on the snowfall process), and we compare the calculated winter SCF with the observed winter SCF. We set the snow density to 200 kg/m³ in the calculations, and add the topographic factors $\sqrt{\frac{1.000SWE}{1.000SWE + \epsilon + 0.15\sigma}}$ (Roesch et al., 2001) and $\left(\frac{SDP}{SDP + \epsilon + 0.0002 - \sigma}\right)^a$ (Li et al., 2019) to five SCF schemes to quantify the influence of topographic factors on the winter SCF calculation.

Based on the above, we also perform 0.1° modeling over the TP (75°–105°E, 25°–40°N) from 1 January 2001 to 31 December 2015 (using the year 2000 for the spin-up period) using SSiB3. We conduct 12 simulations, as shown in Table 1. In the CTL experiment, we evaluate six SCF schemes (MO94, BO96, SX01, NY07, SL12, and LI19) without considering topography. In the TOPO experiment, to investigate the sensitivity of the SCF simulations to the topography and optimize the SCF simulations, we also add the topographic factor of LI19T to MO94, BO96, SX01, and NY07 and obtain the MO94T, BO96T, SX01T, and NY07T schemes. We also evaluate

MIAO ET AL. 5 of 18



the simulation effects of MO94T, BO96T, SX01T, NY07T, SL12T, and LI19T. In the TOPO experiment, a 200 m limitation of SDtopo is added to all the schemes (if SDtopo is larger than 200 m, set it to 200 m), which is drawn from the observations in Section 3.1. Notably, we do not use the topographic factor of Roesch et al. (2001) because it leads to a significant overcorrection in the pre-experimental simulations. To optimize the SCF simulations, we only use the topographic factor of Li et al. (2019) in the TOPO experiment.

In addition to the above 12 simulations described above and shown in Table 1, we also remove the limitation of SDtopo in SX01T to obtain SX01T-no200 as a comparative experiment in Section 3.3 to quantify the influence of the SDtopo limitation.

It should be noted that all the spatial average results in this paper are only through spatial arithmetic averaging, and do not consider different area weights due to latitude changes.

3. Results

3.1. Influence of Topography on SCF Over the TP From Satellite Observations

To investigate whether the SCF schemes in the CTL experiment can well represent the SCF over the TP, we calculate the SCF using the 0.1° SDP satellite data based on five schemes (SL12 is excluded because it is calculated based on the snowfall process). Here, we set the snow density (ρ) to 200 kg/m³ and set the ground roughness (r) to 0.01 m. A comparison of the five SCF schemes is shown in Figure 2. There is a great discrepancy among the five schemes. For a certain SDP, the calculated SCF of SX01 tends to be the largest, while that of NY07 is the smallest. For example, when the SDP is 2 cm, the calculated SCF is 66.67% for MO94, 40% for BO96, 66.40% for YA97/Li19, 100% for SX01%, and 38.00% for NY07. The discrepancy in SCF schemes will lead to a large discrepancy in SCF simulations.

Over the TP, snow cover is mainly distributed on the southeastern and border of the TP in winter (Figures 3a and 3b), where the topography is quite complex. From 2011 to 2015, the regional average winter SCF is 16.84%, and the mean SDP is 2.60 cm. To quantify the difference among five SCF schemes, we compare the calculated SCF and observed SCF from the satellite data in winter from 2011 to 2015, and the spatial distribution of winter mean biases between the calculated SCF and observed SCF is shown in Figure 3. All the calculated SCFs show an overestimation compared to the observed SCF in most areas of the TP, especially in the mountainous areas rich in snow. For example, the SCF bias (calculated SCF minus observed SCF) in the northwestern TP can exceed 50% (SCF equal to 100% means the grid is fully covered by snow). All five SCF schemes underestimate the SCF in the flat areas of the western TP, where there is a significant discrepancy between SCF and SDP observations (Figures 3a and 3b). The SX01 scheme has the largest overestimation of SCF (regional average bias is 29.26%), followed by MO94 (23.23%), LI19 (23.56%), BO96 (16.83%), and NY07 (13.69%) has the smallest overestimation. Among the five schemes, the BO96 and NY07 tend to underestimate the SCF in the flat areas of the TP. This size relationship corresponds to that in Figure 2.

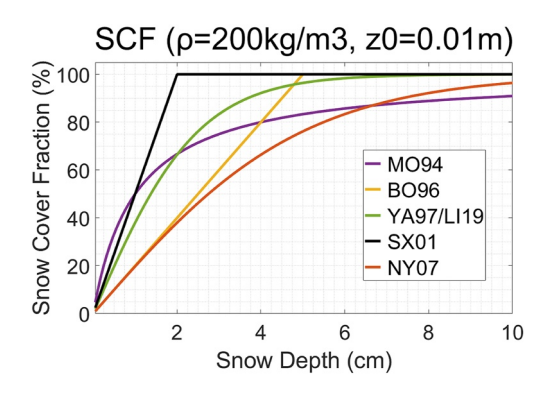


Figure 2. The sketch map of five snow cover fraction (SCF) schemes without consideration of topography based on the formulas (the ground roughness Z_{0g} is set to 0.01 m, the melting factor m is set to 1.0, and the snow density is set to 200 kg/m³).

To further investigate the relationship between the SCF biases and topography, we divide the TP into regions and obtain the regional mean SCF biases. The TP is divided into five regions with SDtopo values between 0 and 100 m, 100–200 m, 200–300 m, 300–400 m, and >400 m. As shown in Table 2, the regional mean results are consistent with the spatial distribution results. The percentage bias of SCF (PBSCF) is also shown in the table, which is the regional mean SCF bias (calculated SCF minus observed SCF) divided by the regional mean observed SCF. All five schemes overestimate the winter SCF to varying degrees, and the PBSCF for the five schemes all increase as SDtopo increases. For example, the PBSCF of SX01 increases from 101.09% in the areas where SDtopo is within 0–100 m, to 198.49% in the areas where SDtopo is within 200–300 m. This suggests that topography complexity significantly affects the snow distribution, causing the overestimation of SCF for five empirical schemes without topography, and the influence of topography complexity on SCF tends to be greater as SDtopo increases.

MIAO ET AL. 6 of 18



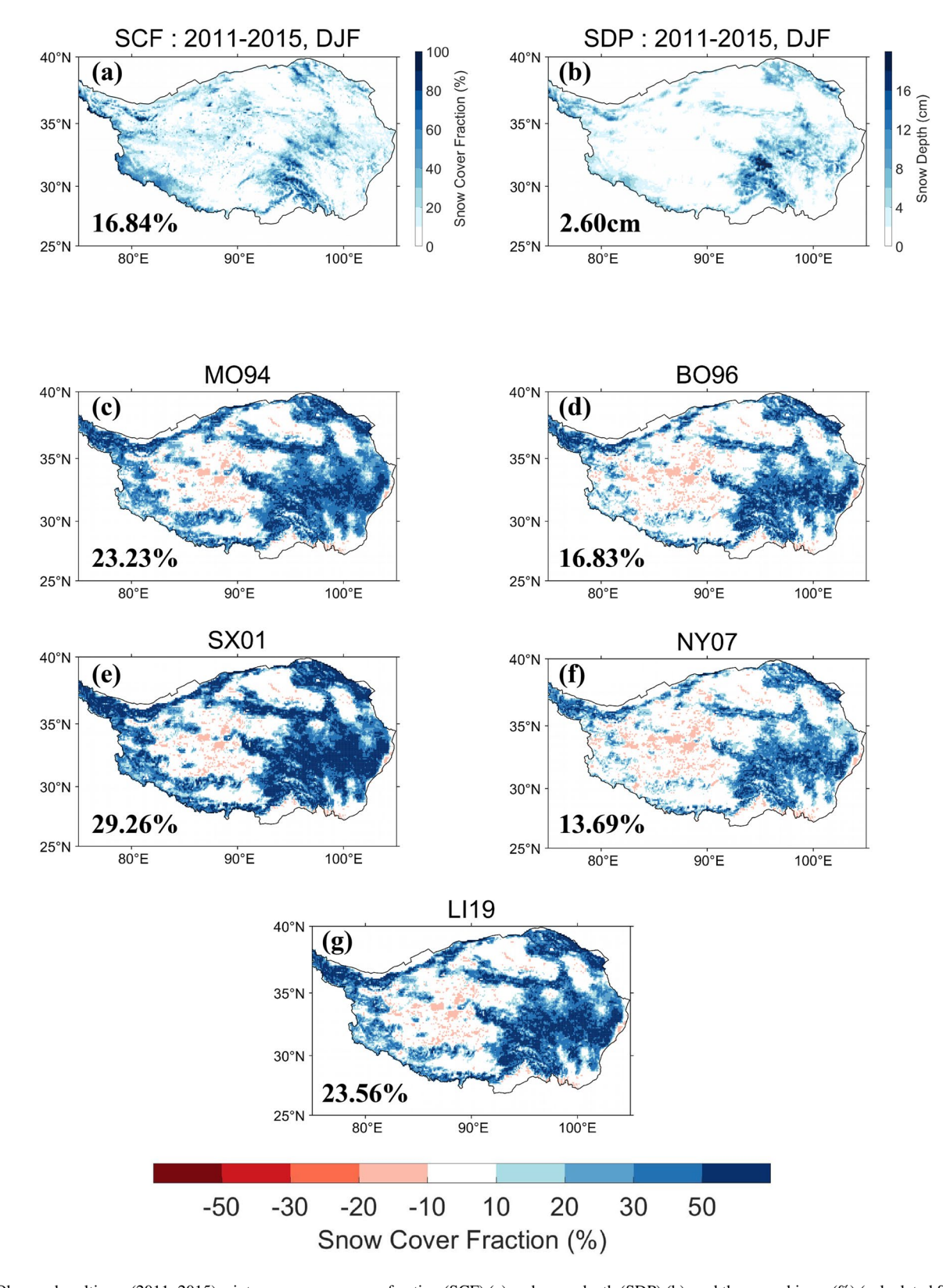


Figure 3. Observed multiyear (2011–2015) winter mean snow cover fraction (SCF) (a) and snow depth (SDP) (b), and the mean biases (%) (calculated SCF minus observed SCF) of (c) MO94, (d) BO96, (e) SX01, (f) NY07, and (g) LI19. The regional average values are shown in the lower-left corner of the plot.

MIAO ET AL. 7 of 18

Table 2
The Spatial Average of Observed Winter Snow Cover Fraction (SCF; %) at Different Standard Deviation of Topography (SDtopo) Ranges (m), and the Biases (Percentage Biases) of the Calculated Winter SCF (%) of the Five Schemes at Different SDtopo Ranges (m)

SDtopo (m)	0–100	100–200	200-300	300–400	>400
MO94—OBS	9.53 (79.73%)	25.19 (147.06%)	32.17 (157.89%)	32.03 (155.68%)	30.53 (145.85%)
BO96—OBS	3.46 (28.92%)	17.55 (102.44%)	25.61 (125.71%)	26.58 (129.19%)	26.02 (124.31%)
SX01—OBS	12.09 (101.09%)	31.45 (183.62%)	40.44 (198.49%)	40.58 (197.27%)	39.32 (187.82%)
NY07—OBS	2.07 (17.28%)	14.38 (83.95%)	21.41 (105.05%)	22.07 (107.27%)	21.24 (101.48%)
LI19—OBS	8.23 (68.87%)	25.10 (146.53%)	33.58 (164.78%)	34.05 (165.52%)	33.07 (157.99%)
OBS	11.96	17.13	20.38	20.57	20.93

However, the increase in PBSCFs starts to slow down after SDtopo reaches 200 m in Table 2, and there is even a small decrease after SDtopo reaches 300 m. Still taking SX01 as an example, the PBSCF of SX01 decreases from 198.49% in the areas where the SDtopo is in the range of 200–300 m, to 197.27% for SDtopo in the range of 300–400 m and then to 187.82% for SDtopo larger than 400 m. To describe this process more intuitively, we make a line chart of PBSCF versus SDtopo. We take a small window (10 m) of SDtopo and make a spatial average of bias. As shown in Figure 4, the lines of the five SCF schemes show a consistent tendency. The PBSCF increases as SDtopo when SDtopo is less than 200 m, but it tends to fluctuate around a value when SDtopo is larger than 200 m. From Figure 1, the areas where SDtopo is greater than 200 m are mostly located in the mountainous areas of the northwestern and southeastern TP. These areas are rich in snow in winter, so the influence of topography on SCF tends to be more important in these areas.

The PBSCFs at the starting point of the lines (the minimum SDtopo) are used to assess the applicability of five schemes in the flat areas. The PBSCFs of BO96 and NY07 are both less than -30% at the starting point; therefore, using these two schemes will lead to a negative SCF simulation bias in the flat areas. In contrast, LI19 behaves better at the starting point with a very small PBSCF. It should be noted that the above results cannot represent the effect of these SCF schemes in actual simulations, because we set the snow density to a constant (200 kg/m^3) which has a great influence on the results, especially for SX01 and NY07. In actual simulations, the uncertainties in the snow models and meteorological forcing data lead to an uncertain result.

As mentioned above, a great influence of topography on winter SCF exists over the TP, and ignoring the topography leads to a great bias of simulated winter SCF. Different from previous studies, we find that the influence of topography on SCF does not monotonically change with topography complexity based on satellite observations. When the SDtopo increases from 0 m, the PBSCF increases correspondingly; however, when the SDtopo reaches a tipping point (200 m), the influence of topography on SCF no longer grows.

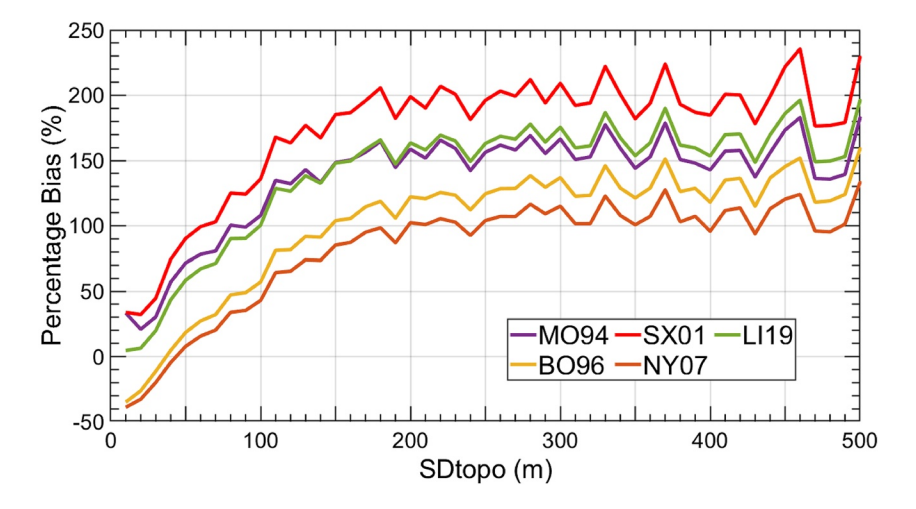


Figure 4. The relationship between the standard deviation of topography (SDtopo; m) and percentage bias (%) of the calculated winter snow cover fraction of the five schemes.

MIAO ET AL. 8 of 18



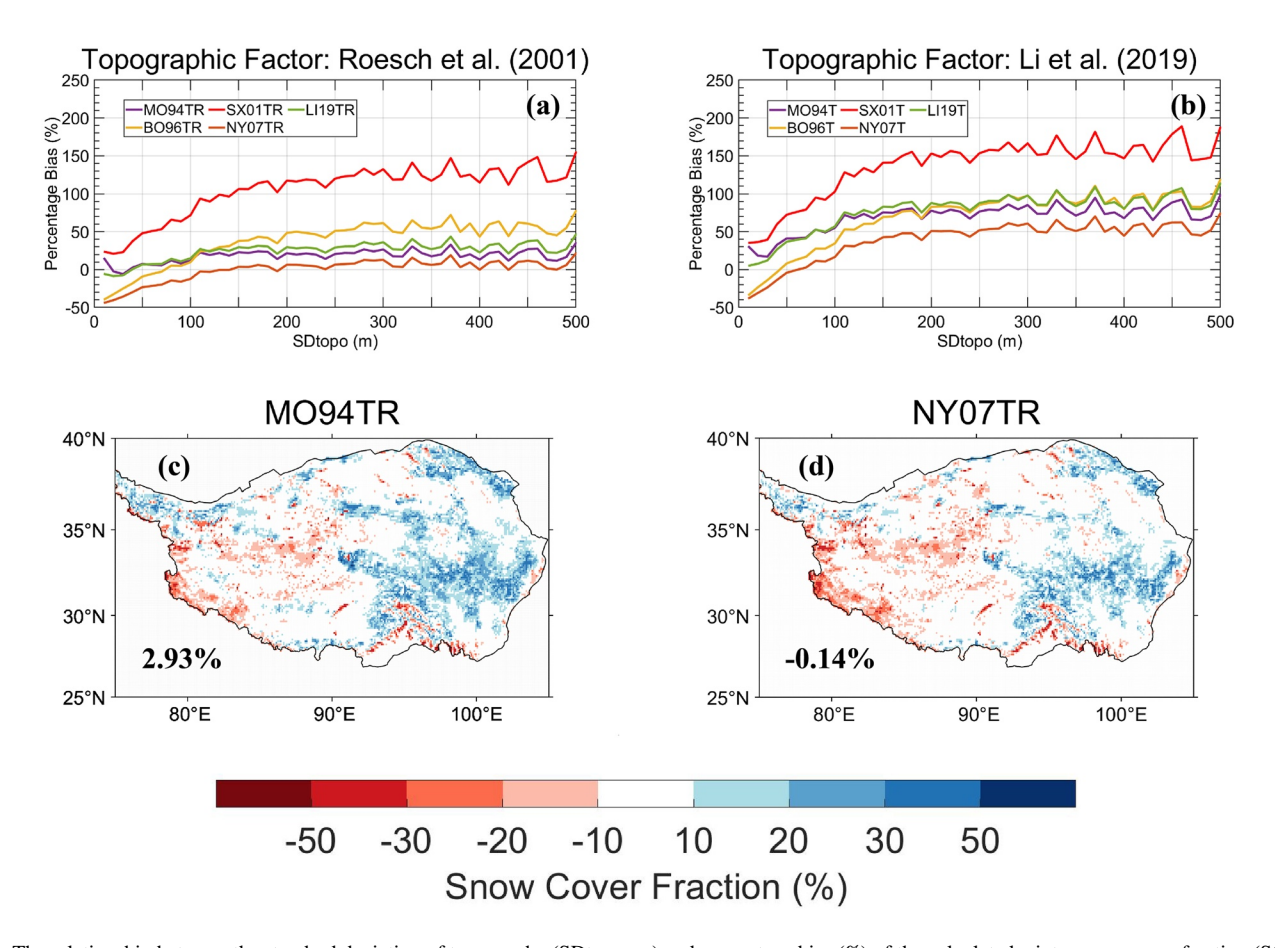


Figure 5. The relationship between the standard deviation of topography (SDtopo; m) and percentage bias (%) of the calculated winter snow cover fraction (SCF) of the five schemes with topographic factors of (a) Roesch et al. (2001) and (b) Li et al. (2019). Multiyear (2011–2015) winter mean biases (%) (calculated SCF minus observed SCF) of (c) MO94TR and (d) NY07TR. The regional average values are shown in the lower-left corner of the plot.

To reduce the bias in the calculated SCF, we incorporate the topographic factor and 200 m limit for SDtopo into the original schemes. Here, we add the topographic factors $\sqrt{\frac{1.000SWE}{1.000SWE + \varepsilon + 0.15\sigma}}$ (Roesch et al., 2001) and

 $\left(\frac{\text{SDP}}{\text{SDP}+\varepsilon+0.0002 \cdot \sigma}\right)^a$ (Li et al., 2019) to five SCF schemes to investigate the relationship between PBSCF and SDtopo

(Figures 5a and 5b). Using the topographic factors indeed reduces the PBSCF to some extent. However, the correction of calculated SCF by the topographic factor of Li et al. (2019) is not adequate (Figure 5b), and the PBSCFs of five schemes are still larger than 50% when SDtopo is larger than 200 m. In contrast, the topographic factor of Roesch et al. (2001) performs better. In Figure 5a, the PBSCFs of the five schemes are significantly reduced to within $\pm 50\%$, except for the SX01 scheme. Among the five schemes, MO94TR (the "TR" indicates that the scheme includes the topographic factor of Roesch et al. (2001)) and NY07TR behave better. MO94TR behaves better in flat areas (SDtopo <100 m) but has an overestimation by 20% when SDtopo is greater than 100 m. NY07TR has a significant underestimation when SDtopo is lower than 100 m but behaves better when SDtopo is greater than 100 m with a positive bias lower than 20%.

To further select the best scheme to quantify the topographic effect on SCF, we derive the spatial distribution of SCF bias based on MO94TR and NY07TR schemes (Figures 5c and 5d). Compared to the results in Figure 3, the positive SCF bias has been greatly reduced. Compared with MO94TR, NY07TR has a larger underestimation in the central and western TP and a smaller overestimation in the eastern and southeastern TP. The regional mean bias of MO94TR is 2.93% while it is -0.14% for NY07TR. We also perform statistical analysis to further compare MO94TR with NY07TR. The MAE is reduced from 25.45% for MO94% to 9.70% for MO94TR, while the RMSE is reduced from 32.19% to 12.98%. For NY07 and NY07TR, the MAE and RMSE are reduced from 17.36% to 24.09%–8.78% and 12.11%, respectively. Both MO94TR and NY07TR have obvious optimization of

MIAO ET AL. 9 of 18



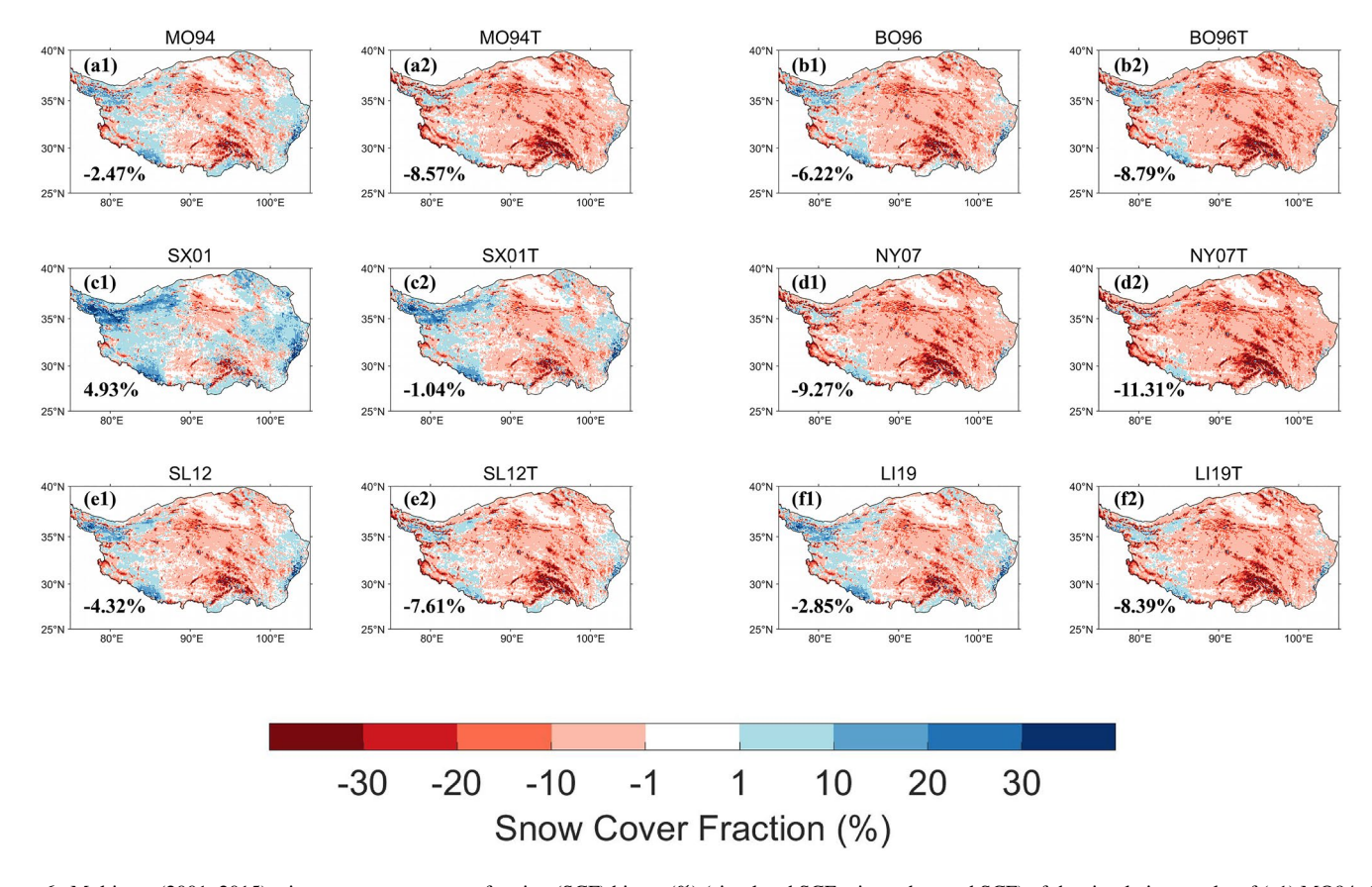


Figure 6. Multiyear (2001–2015) winter mean snow cover fraction (SCF) biases (%) (simulated SCF minus observed SCF) of the simulation results of (a1) MO94, (a2) MO94T, (b1) BO96, (b2) BO96T, (c1) SX01, (c2) SX01T, (d1) NY07, (d2) NY07T, (e1) SL12, (e2) SL12T, (f1) L119, and (f2) L119T. The regional mean values are shown in the lower-left corner of the plot.

SCF estimation, and NY07TR shows a better performance compared with the observations. Taking NY07 and NY07TR as examples to quantify the actual influence of topography on SCF simulations, the regional mean bias is reduced from 13.69% to -0.14%. Given the fact that the observed regional mean SCF is 16.84% in winter, this means that the large SCF bias is almost eliminated by introducing the topographic factor.

Following the above results based on observations, we could reasonably assume that the topographic effect also exists in SCF simulations. In the next section, we will optimize the SCF simulations by considering topographic effects in SSiB3 simulations and further quantify their impact on the surface energy budget simulations.

3.2. Regional Simulation Results of the Different SCF Schemes

To evaluate the simulation effects of different SCF schemes without consideration of the topographic factor in the actual simulations, we conduct six simulations with a 0.1° spatial resolution (Table 1, CTL experiment), and the winter mean SCF biases are shown in Figures 6a1–6f1.

Different schemes have consistent underestimation in the mountainous areas of the southeastern and northeastern TP, and this underestimation can be lower than -30%. A consistent overestimation exists in the northwestern and southwestern TP. Significant differences also exist among the six SCF schemes. As shown in Figure 6c1, SX01 greatly overestimates SCF, especially in the northwestern TP where the bias is greater than 30%. Moreover, NY07 greatly underestimates SCF over the TP (Figure 6d1). Among the other four schemes, MO94 performs a better simulation in the flat areas of the central TP, while BO96 underestimates the SCF in most of the flat areas. In the northwest and border of the TP, the simulated SCFs of the four remaining schemes are all overestimated.

The observed regional mean SCF is 17.05%, and the simulated SCF biases of the six schemes are -2.47% for MO94%, -6.22% for BO96, 4.93% for SX01%, -9.27% for NY07%, -4.32% for SL12%, and -2.85% for LI19

MIAO ET AL. 10 of 18



Table 3

The Spatial Average of Observed Winter Snow Cover Fraction (SCF; %) at Different Standard Deviation of Topography (SDtopo) Ranges (m), and the Biases (Percentage Biases) of the Simulated SCF (%) of the Six Schemes in the CTL Experiment, SX01T and SX01T-no200 (SX01T Scheme Without 200 m Limitations of SDtopo) at Different SDtopo Ranges (m)

SDtopo (m)	0–100	100–200	200-300	300–400	>400	Total
MO94—OBS	-1.58 (-18.01%)	-0.12 (-1.51%)	-0.07 (-1.05%)	0.31 (7.31%)	0.15 (1.91%)	-0.28 (-3.84%)
BO96—OBS	-5.00 (-56.98%)	-3.62 (-46.85%)	-2.72 (-42.10%)	-2.23 (-52.39%)	-2.30 (-30.05%)	-3.26 (-44.48%)
SX01—OBS	2.73 (31.17%)	4.27 (55.33%)	4.03 (62.23%)	4.89 (114.71%)	3.60 (46.94%)	3.83 (52.25%)
NY07—OBS	-6.26 (-71.39%)	-5.01 (-64.86%)	-4.17 (-64.39%)	-3.01 (-70.46%)	-3.69 (-48.17%)	-4.58 (-62.38%)
SL12—OBS	-3.67 (-41.81%)	-2.22 (-28.72%)	-1.48 (-22.92%)	-1.30 (-30.47%)	-0.57 (-7.37%)	-1.87 (-25.49%)
LI19—OBS	-2.37 (-26.97%)	-1.16 (-15.04%)	-0.79 (-12.17%)	-0.35 (-8.32%)	-0.31 (-4.10%)	-1.04 (-14.15%)
SX01T—OBS	0.38 (4.30%)	-0.20 (-2.58%)	-0.68 (-10.49%)	0.53 (12.47%)	-0.18 (-2.35%)	-0.10 (-1.33%)
SX01T-no200—OBS	-0.38 (4.30%)	-0.20 (-2.58%)	-0.97 (-15.01%)	-0.36 (-8.52%)	-1.26 (-16.44%)	-0.50 (-6.86%)
OBS	8.77	7.72	6.47	4.27	7.67	7.33
Number of stations	19	28	18	10	24	99

Note. The results are based on the observations and simulations at the location of China Meteorological Administration stations.

(Figure 6). Consistent negative biases exist in these SCF schemes except for SX01, which is mainly due to the systematic underestimation in the southeastern TP. According to previous studies, these consistent biases may come from uncertainties in the winter precipitation forcing data (Jiang et al., 2020; Y. Gao et al., 2020). The underestimated precipitation in winter leads to a great underestimation of SCF. Furthermore, the uncertainties in the SSiB3 model or the observation data can also lead to this bias.

As shown in Table 1, we also conduct six corresponding simulations in the TOPO experiment to examine the sensitivity of the simulation results to topography. Before the TOPO experiment, we perform the pre-experimental simulations to test the applicability of two topographic factors in the actual simulations using SSiB3 forced by CMFD. The results show a significant underestimation using the topographic factor of Roesch et al. (2001). Therefore, here, we only use the topographic factor of Li et al. (2019) to account for the topographic effect in the actual simulations. Among these simulations, we restore the topographic factor of the SL12 and LI19, and add the topographic factor of LI19T to the other four schemes.

In the TOPO experiment, we set the SDtopo to 200 m when SDtopo is greater than 200 m. The addition of the topographic factor reduces the simulated SCFs. For example, the addition of the topographic factor greatly reduces the positive SCF bias of SX01 in the northwestern TP (Figure 6c1 and 6c2). The spatial mean SCF bias of SX01 is reduced from 4.93% to -1.04%. The MAE of six schemes changes from 8.90%, 9.90%, 10.97%, 11.02%, 9.41%, and 9.13%–10.64%, 11.02%, 9.59%, 12.36%, 10.13%, and 10.66%, while the RMSE changes from 13.71%, 15.04%, 16.32%, 16.60%, 14.52%, and 13.99%–16.45%, 16.39%, 14.45%, 18.30%, 15.87%, and 16.27%. This indicates that the simulation results are sensitive to the topographic factor. However, the regional simulation results are greatly influenced by the systematic bias, the regional mean bias, MAE, and RMSE values indicate that the simulations tend to be worse except for SX01. The systematic bias prevents us from accurately examining the effect of topography on SCF. Notably, CMFD forcing data incorporated in-situ data from CMA stations, and the forcing data at the location of CMA stations are more reliable and realistic. To narrow the uncertainty induced by forcing data to the greatest extent, the following analysis will be based on simulation results at the location of the CMA stations.

3.3. Simulation Result at the Location of CMA Stations

As shown in Figure 1, there are 99 CMA stations in our study area, and we extract the simulation results of the nearest grid points based on the coordinates. These grids are also divided into five regions based on the SDtopo to obtain the average results.

Table 3 shows the average SCF biases (PBSCF) of six SCF schemes in the CTL experiment, SX01T and SX01T-no200 (Other schemes with the topographic factor in the TOPO experiment are not shown due to their

MIAO ET AL. 11 of 18



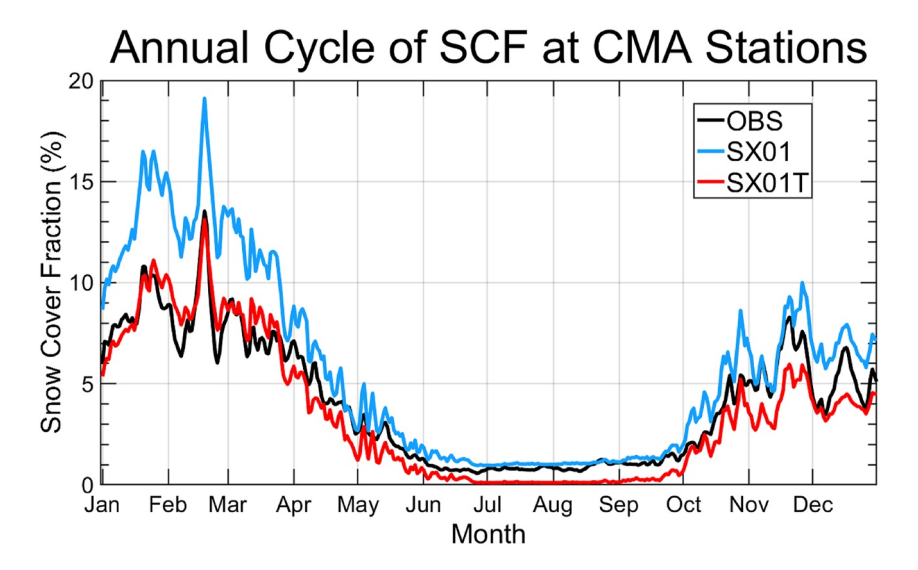


Figure 7. Multiyear (2001–2015) average annual cycle of the observed snow cover fraction (SCF) and simulated SCF of SX01 and SX01T at the location of China Meteorological Administration (CMA) stations.

great underestimation of SCF). The SX01T-no200 scheme removes the limitation that SDtopo is not greater than 200 m in the SX01T scheme, which is for comparison with the SX01T scheme to quantify the influence of the 200 m limitation. In Table 3, the PBSCFs of the six schemes in the CTL experiment consistently increase with SDtopo, and this increase tends to slow down when SDtopo is greater than 200 m, which corresponds to the conclusions in Section 3.1. Among the six schemes in the CTL experiment, BO96, NY07, SL12, and LI19 all underestimate the SCF in all regions. MO94 underestimates the SCF when SDtopo is less than 300 m and overestimates it when SDtopo is greater than 300 m. The monotonic change in SCF bias leads to a good overall simulation with a negative bias of -0.28%. Besides, SX01 greatly overestimates the SCF in all ranges of SDtopo with an overall positive bias of 3.83%. Overall, MO94 performs the best simulation among the six schemes, but it does not consider topography and greatly underestimates the SCF in flat areas.

Based on the SX01 scheme and the topographic factor of LI19T, we obtain SX01T with a 200 m limitation of SDtopo. SX01T significantly reduces the bias of SX01 in all ranges of SDtopo. The winter SCF bias has been reduced from 3.83% to -0.10%. No matter in flat areas or mountainous areas, SX01T has good performance. To investigate the influence of the 200 m limitation of SDtopo, we remove the limitation and obtain the SX01T-no200 scheme to simulate the SCF. Compared to SX01T-no200, SX01T shows better performance when SDtopo is greater than 200 m, especially when SDtopo is greater than 400 m. The 200 m limitation of SDtopo avoids the overcorrection of topography-induced biases and makes the simulation more accurate.

In addition, the seasonal variation in snow cover is also very important. In Figure 7, the multiyear average annual cycle of SCFs of SX01, SX01T, and the observations are shown. Compared to observations, SX01 and SX01T both well represent the seasonal variation characteristics of TP snow cover. However, SX01 greatly overestimates SCF. SX01T optimizes the SCF simulation to a certain extent in the three snow seasons of autumn, winter, and spring. Especially from January to March, SX01T greatly reduces the positive bias by approximately 5% in SX01. We also perform a corresponding statistical analysis, and the annual MAE of SX01T is 0.89%, compared to 1.69% of SX01. The annual RMSE of SX01T is 1.03%, while the RMSE of SX01 is 2.46%. In winter, the MAEs of SX01 and SX01T are 3.79% and 0.89%, respectively; the RMSEs of SX01 and SX01T are 4.14% and 1.04%, respectively. The statistical analysis results indicate that the simulation result of SX01T is much better than that of SX01. The SCF simulations at the location of the CMA stations are optimized by considering the effect of topography on the SCF and setting a 200 m limitation for SDtopo.

3.4. Effect on Land Surface Energy Balance Simulations

The SCF simulation directly influences the surface shortwave albedo simulation. In snow models, SCF represents the gridded area percentage of snow cover, which is applied as a weighted coefficient of snow albedo in surface

MIAO ET AL. 12 of 18



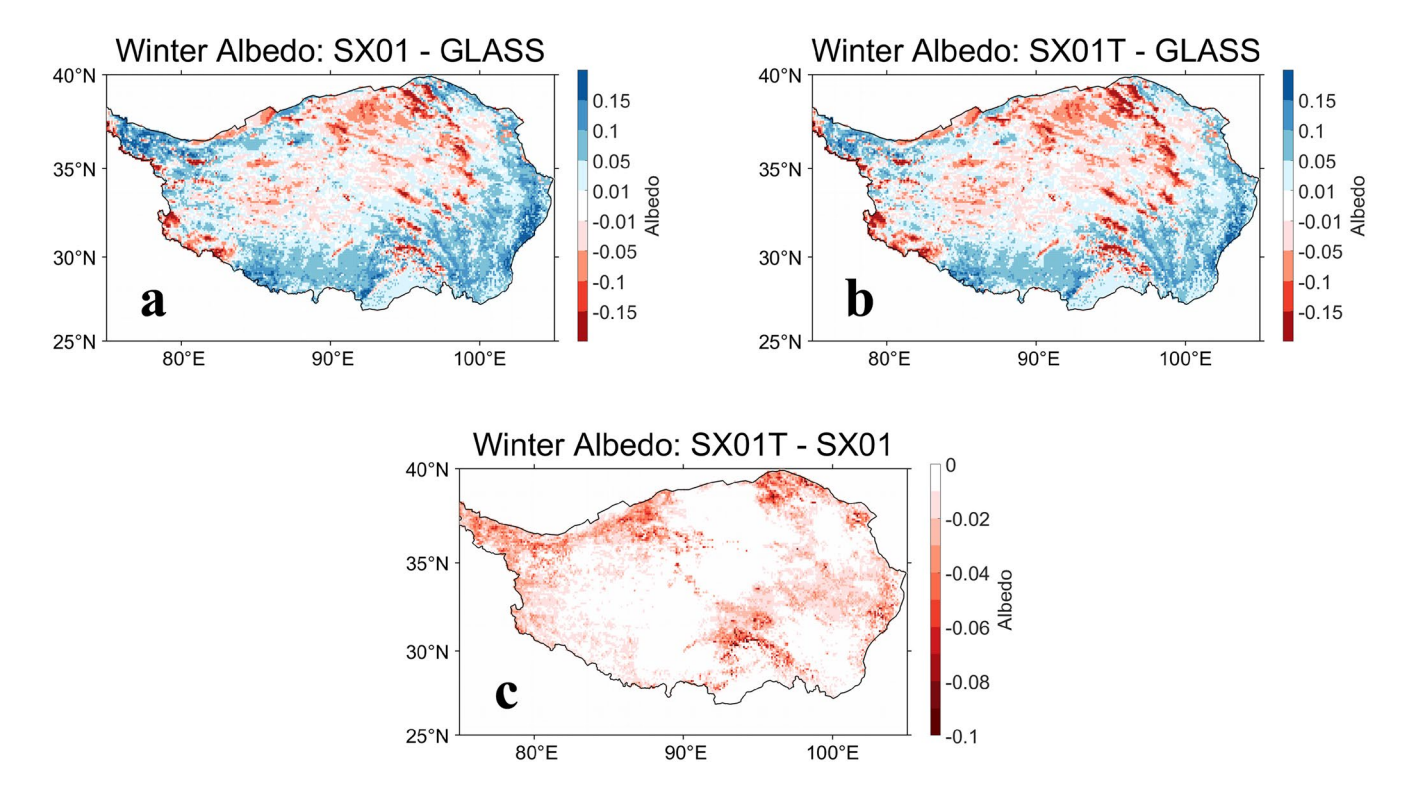


Figure 8. Multiyear (2001–2015) winter mean surface albedo biases of (a) SX01-GLASS, (b) SX01T-GLASS, and (c) SX01T-SX01.

albedo calculations. SCF mainly influences the surface albedo in snow seasons (from September to next May). We evaluate the effects of the modification of SCF schemes on albedo simulations in winter, compared with the GLASS shortwave albedo product. Figure 8 shows the albedo biases of SX01, SX01T, and the difference between SX01T and SX01 (SX01T minus SX01). Consistent albedo biases occur on the southern, southeastern, and northern TP, and these biases may come from the uncertainties in the forcing data or the model. Compared with SX01, SX01T reduces the positive albedo biases in the northwestern, eastern, and border regions of the TP, and the reduction in bias can reach 0.1 in mountainous areas, which will greatly influence the land surface radiation budget.

To better investigate the effects of SCF schemes on the simulated albedo, we calculate the spatial mean results. The mean winter albedo bias is reduced from 0.020 for SX01 to 0.007 for SX01T over the TP, with a maximum reduction located in the southeastern TP by -0.133. The MAE is reduced from 0.054 for SX01 to 0.050 for SX01T, while the RMSE is reduced from 0.070 to 0.067. At the location of CMA stations, the winter bias is reduced from 0.042 to 0.034, and the MAE and RMSE are reduced from 0.052 to 0.062 for SX01, to 0.046 and 0.055 for SX01T, respectively. The reduction in positive winter albedo bias leads to an increase in simulated income shortwave radiation and then influences the land surface energy balance simulations.

To show the influence of topography on land surface energy balance simulation in winter, we output the LST to compare with observations (Figure 9). According to Figure 9a, the simulated LST is much lower than the observation in the southwestern, northwestern, and border regions of the TP, and the negative bias can be below –6 K. By adding the topographic factor, the bias of simulated LST is reduced, especially in the northwestern TP. However, an overestimation exists in the southeastern TP for the SX01 scheme, due to the systematic bias of simulated SCF; the simulated LST is further increased after including the topographic factor. For the entire TP, the LST bias is reduced from –3.33 to –3.04 K. The reduction can reach 3.60 K in the southeastern TP, and it is larger than 1 K in most areas of the northwestern TP. The MAE is reduced from 3.74 K for SX01 to 3.50 K for SX01T, while the RMSE is reduced from 4.38 to 4.11 K. At the location of CMA stations, the bias is reduced from –1.88 to –1.69 K, and the MAE and RMSE are reduced from 2.67 to 3.16 K for SX01 to 2.56 and 3.05 K for SX01T, respectively. This indicates that the bias of simulated LST is reduced by including the topographic factor.

MIAO ET AL. 13 of 18



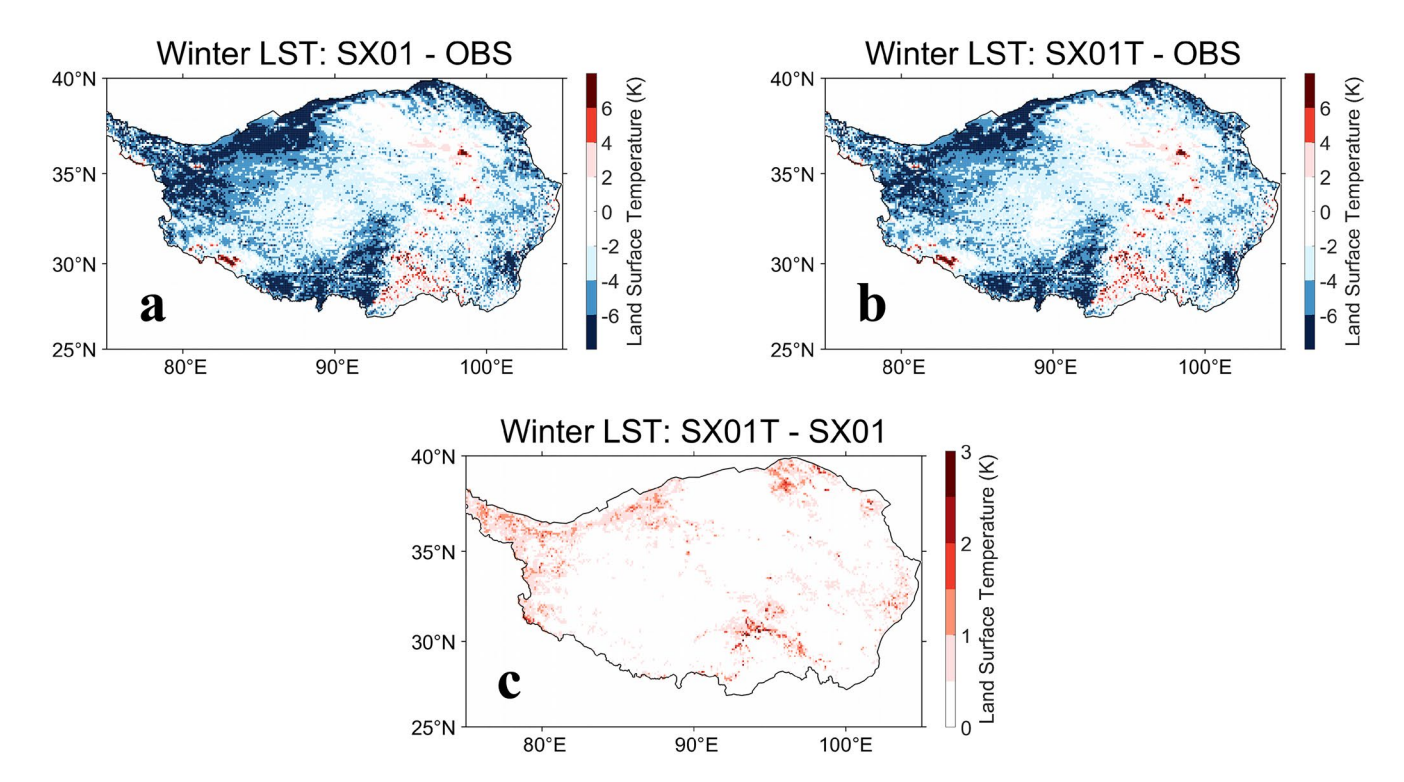


Figure 9. Multiyear (2001–2015) winter mean land surface temperature biases of (a) SX01-OBS, (b) SX01T-OBS, and (c) SX01T-SX01.

In conclusion, the addition of the topographic factor improves the SCF simulation, and in consequence optimizes the land surface energy budget simulation, despite the uncertainty in the forcing data or the model that makes the interpretations not straightforward.

4. Discussion

The subgrid snow cover distribution is a key process in snow models and greatly influences the land surface energy balance (Liston, 2004; Liston & Elder, 2006). Subgrid topography has a great influence on snow-related processes. Complex topography can accelerate the snowmelt of south-facing slopes and cause nonuniform snow cover distributions (Roesch et al., 2001). Lehning et al. (2008) indicated that the inhomogeneous snow distributions found in mountainous areas result from the interactions of wind and precipitation with (snow) surfaces over topography. Mott et al. (2018) also indicated that topography can cause non-uniform distribution of snowfall in mountainous areas. In climate simulations and land surface simulations, the resolution of models is often low, which also means that topographic effects at the kilometer or even hundred-meter scale cannot be reflected in the input data. Therefore, the subgrid processes need to be described by the parameterization schemes or submodules. In this study, we use the gridded SDtopo to state the complexity of subgrid topography. The SDtopo distribution over the TP is shown in Figure 1, and it indicates that the subgrid topography over the TP is quite complex, which can greatly influence the subgrid snow cover distribution. To improve the snow cover simulations, we add the topographic factor to include the topographic effects based on the analysis of satellite observations. In addition to SDtopo, the squared slope has been used to represent subgrid topography in recent research (Helbig, Bühler, et al., 2021; Helbig, Schirmer, et al., 2021; Helbig et al., 2015; Skaugen & Melvold, 2019). Helbig, Bühler, et al. (2021) performed a correlation analysis for subgrid SDP variability with various commonly applied topographic characteristics, and a squared slope-related parameter shows a better correlation than SDtopo with subgrid spatial SDP variability. Using the slope-related parameter to represent the subgrid topography is more realistic for snow processes. It offers us a new method to account for topographic effects on TP snow cover simulations. The scheme of Helbig, Bühler, et al. (2021) was developed and evaluated based on the SDP observations with meter-scale spatial resolution in North America and Europe. However, on the TP, there are only satellite

MIAO ET AL. 14 of 18



observations of SDP with a spatial resolution of kilometer level and sparse in-situ observations of SDP. Due to the lack of high-resolution SDP observations, we are currently unable to evaluate this scheme over the TP.

The overall SCF simulation is significantly improved by considering the influence of topography on SCF in this study. However, uncertainties still exist when simulating seasonal variations in SCF. As shown in Figure 7, the winter SCF is well simulated, but the SCF is underestimated in the snow melting period (from March to May). Previous studies have stressed the importance of seasonal variations in SCF. Niu and Yang (2007) improved the previous scheme (Z. L. Yang et al., 1997) by considering seasonal variations in snow density. Swenson and Lawrence (2012) developed a new SCF parameterization scheme by considering the SCF differences between snow accumulation and snowmelt seasons. Recently, Helbig, Schirmer, et al. (2021) presented an algorithm that describes the seasonal snow cover evolution by tracking the SDP and SWE history over the season and evaluated it with independent SCF data sets. In different seasons, snow properties such as snow density change periodically, and snow cover also has different characteristics in the accumulation and melting periods. Therefore, it is necessary to further optimize SCF simulations by including the seasonal variation of snow cover.

There remain several uncertainties in this study, one of which is the uncertainty of meteorological forcing data. In this study, the CMFD is used as the meteorological forcing data to drive the SSiB3 model. CMFD is a state-of-theart meteorological forcing data incorporating site observations in China and is widely used in research on the TP (B. Wang, Ma, et al., 2020; Jiang et al., 2020; W. Wang, Yang, et al., 2020; Z. Kang et al., 2022). However, uncertainty remains in the CMFD data sets. B. Wang, Ma, et al. (2020) evaluated and corrected the bias between CMFD data and in-situ observations. Y. Gao et al. (2020) indicated that the CMFD underestimates precipitation on the southeastern TP. In this study, we analyze the simulation results at the location of CMA stations to reduce the uncertainty caused by the forcing data, but the influence of forcing data remains.

In addition, there remains uncertainty in the model and the topographic factor. In the land surface model, the snow cover simulation includes many processes such as snow stratification, snow densification, snow melting/refreezing, the aerosols in the snow, and so on. The simulations of these processes determine the final results together. SSiB3 is used for the simulations in this study, and it also has several limitations. For example, the snow albedo is calculated based on an empirical parameterization scheme, which may lead to uncertainties in the energy budget simulations. The stratification scheme is quite simple, which can lead to bias in snow simulations. The SSiB3 model needs to be further optimized based on the observations over the TP. Furthermore, in this study, we use the topographic factor of L119T to account for the topographic effect, and the SCF simulation bias is significantly reduced. However, the parameters in the topographic factor are sensitive to the spatial resolution, and it needs to be further modified over the TP. Due to the limitation of observations, the optimization of snow models and modification of the topographic factor for the whole TP is quite difficult. More in situ observations over the TP and precise satellite observations of snow quantities over mountainous areas are needed, which is essential to better evaluate the snow cover parameterizations and better represent snow cover in land surface models.

This research aims to optimize the SCF simulations using the SSiB3 model. In this context, the "best" SCF parameterization depends on the specific land surface model and atmospheric forcing data. Even though SX01T overestimates the SCF in terms of the observations, it produces the best simulation at the locations of the 99 CMA stations. In the observation, NY07TR is the best SCF scheme. However, we test the NY07TR and other schemes with the topographic factor of Roesch et al. (2001) in pre-experimental simulations, and the results indicate an obvious underestimation. Therefore, NY07TR is no more the best choice for the simulations of SSiB3 forced by CMFD. This is the reason that we take SX01T as an illustration to show the necessity and advantage of including the topographic factor in the numerical experiments.

5. Conclusions

In this study, the influence of topography on SCF simulations in winter is investigated using satellite observations and numerical simulations. A topographic factor and a limitation of the topographic effect are added to the original SCF scheme to account for the topographic effect on the SCF simulations. The conclusions are described below.

MIAO ET AL. 15 of 18



The analysis of satellite observations indicates that SCF simulation biases increase with the topography complexity, and this increasing trend slows down when the SDtopo is greater than 200 m. Adding the topographic factor to the original SCF schemes and setting a 200 m limitation for SDtopo, the bias of calculated SCF is significantly reduced. For the best scheme NY07TR in the observations, the regional mean bias is reduced from 13.69% to -0.14%.

In the SSiB3 simulations, applying the topographic factor greatly reduces the simulated SCF. To narrow the uncertainty that may be caused by the forcing data, we analyze the simulations at the locations of the CMA stations. As a result, the winter SCF bias is reduced from 3.83% to -0.50% by adding the topographic factor, and the bias is further reduced from -0.50% to -0.10% by setting a limitation of SDtopo.

The improvement in SCF stimulation contributes to better simulations of surface albedo and LST. The mean albedo bias in winter is reduced from 0.020 to 0.007 over the whole TP, with a maximum reduction located in the southeastern TP by -0.133. At the same time, the LST bias is reduced from -3.33 to -3.04 K, with a maximum reduction located in the southeastern TP by 3.60 K.

In this paper, snow cover and land surface energy budget simulations are improved by accounting for topographic effects on SCF, despite the uncertainties in forcing data and model that make the interpretations not straightforward. It offers us a good reference to reduce the "cold bias" in near-surface air temperature simulation in land-atmosphere coupled models in winter. To better account for the topographic effect, more accurate in-situ and satellite observations are needed to modify the topographic factors and optimize the land surface models. Furthermore, the seasonality of SCF should be taken into account in future work.

Data Availability Statement

The meteorological forcing data China Meteorological Forcing Dataset is available at http://data.tpdc.ac.cn/en/data/8028b944-daaa-4511-8769-965612652c49/, provided by the National Tibetan Plateau Data Center. The daily cloudless Moderate Resolution Imaging Spectroradiometer (MODIS) snow area ratio data set of the QTP is downloaded at https://data.tpdc.ac.cn/en/data/94a8858b-3ace-488d-9233-75c021a964f0/. The 0.05° snow depth data set for Tibetan Plateau is available at https://data.tpdc.ac.cn/en/data/0515ce19-5a69-4f86-822b-330aa11e2a28/. The land cover data (MCD12C1v006) are available at https://doi.org/10.5067/MODIS/MCD12C1.006. The Global Land Surface Satellite albedo products were developed by the National Earth System Science Data Center, National Science and Technology Infrastructure of China (http://www.geodata.cn/. The Digital Elevation Model data are available at https://data.tpdc.ac.cn/en/data/ddf4108a-d940-47ad-b25c-03666275c83a/ and are provided by the NASA. The leaf area index data are provided by the Land-Atmosphere Interaction Group at the Sun Yat-sen University (https://globalchange.bnu.edu.cn/research). The MODIS daily land surface temperature product is available at https://modis.gsfc.nasa.gov/data/dataprod/mod11.php. The code of Simplified Simple Biosphere Model version 3 and necessary input data used in this work are available at https://doi.org/10.5281/zenodo.6778122.

Acknowledgments

The authors thank Yongming Xu from the Nanjing University of Information Science and Technology for helping with processing the land surface temperature remote sensing data. This study was jointly supported by the Second Tibetan Plateau Scientific Expedition and Research Program (STEP) (Grant No. 2019QZKK0103), the Strategic Priority Research Program of the Chinese Academy of Sciences (Grant No. XDA2006010104), and the Open Research Fund Program of Plateau Atmosphere and Environment Key Laboratory of Sichuan Province (No. PAEKL-2022-K01).

References

- Bian, Q., Xu, Z., Zheng, H., Li, K., Liang, J., Fei, W., et al. (2020). Multiscale changes in snow over the Tibetan Plateau during 1980–2018 represented by reanalysis data sets and satellite observations. *Journal of Geophysical Research: Atmospheres*, 125(19), e2019JD031914. https://doi.org/10.1029/2019JD031914
- Bonan, G. B. (1996). A land surface model (LSM version 1.0) for ecological, hydrological, and atmospheric studies: Technical description and user's guide. NCAR Technical Note NCAR/TN-417+STR, 150. https://doi.org/10.5065/D6DF6P5X
- Chen, A., Hu, S., Meng, W., & Bian, L. (2015). An assessment on the accuracy of the GLASS albedo products over the Tibetan Plateau. Acta Meteorologica Sinica, 73(6), 1114–1120. https://doi.org/10.11676/qxxb2015.074
- Chen, A., Meng, W., Hu, S., & Bian, L. (2020). Comparative analysis on land surface albedo from MODIS and GLASS over the Tibetan Plateau. Transactions of Atmospheric Sciences, 43(5), 932–942. https://doi.org/10.13878/j.cnki.dqkxxb.20171030001
- Chen, X., Liu, Y., & Wu, G. (2017). Understanding the surface temperature cold bias in CMIP5 AGCMs over the Tibetan Plateau. Advances in Atmosphere Sciences, 34(12), 1447–1460. https://doi.org/10.1007/s00376-017-6326-9
- Cui, T., Li, C., & Tian, F. (2021). Evaluation of temperature and precipitation simulations in CMIP6 models over the Tibetan Plateau. Earth and Space Science, 8(7), e2020EA001620. https://doi.org/10.1029/2020EA001620
- Dickinson, R., Henderson-Sellers, A., & Kennedy, P. J. (1993). Biosphere atmosphere transfer scheme (BATS) version le as coupled to the NCAR community climate model. NCAR Technical Note, 72. https://doi.org/10.5065/D67W6959
- Douville, H., Royer, J. F., & Mahfouf, J. F. (1995). A new snow parameterization for the Meteo-France climate model. Part II: Validation in a 3-D GCM experiment. Climate Dynamics, 12(1), 37–52. https://doi.org/10.1007/BF00208761

MIAO ET AL. 16 of 18



- Duan, A., Hu, J., & Xiao, Z. (2013). The Tibetan Plateau summer monsoon in the CMIP5 simulations. *Journal of Climate*, 26(19), 7747–7766. https://doi.org/10.1175/JCLI-D-12-00685.1
- Gao, F., He, T., Wang, Z., Ghimire, B., Shuai, Y., Masek, J., et al. (2014). Multiscale climatological albedo look-up maps derived from moderate resolution imaging spectroradiometer BRDF/albedo products. *Journal of Applied Remote Sensing*, 8(1), 083532. https://doi.org/10.1117/1. JRS.8.083532
- Gao, Y., Chen, F., & Jiang, Y. (2020). Evaluation of a convection-permitting modeling of precipitation over the Tibetan Plateau and its influences on the simulation of snow-cover fraction. *Journal of Hydrometeorology*, 21(7), 1531–1548. https://doi.org/10.1175/JHM-D-19-0277.1
- Gao, Y., Xu, J., & Chen, D. (2015). Evaluation of WRF mesoscale climate simulations over the Tibetan Plateau during 1979–2011. *Journal of Climate*, 28(7), 2823–2841. https://doi.org/10.1175/jcli-d-14-00300.1
- Harrison, T. M., Copeland, P., Kidd, W. S. F., & Yin, A. (1992). Raising Tibet. Science, 255(5052), 1663–1670. https://doi.org/10.1126/science.255.5052.1663
- He, J., Yang, K., Tang, W., Lu, H., Qin, J., Chen, Y., & Li, X. (2020). The first high-resolution meteorological forcing dataset for land process studies over China. Scientific Data, 7(1), 25. https://doi.org/10.1038/s41597-020-0369-y
- Helbig, N., Bühler, Y., Eberhard, L., Deschamps-Berger, C., Gascoin, S., Dumont, M., et al. (2021). Fractional snow-covered area: Scale-independent peak of winter parameterization. *The Cryosphere*, 15(2), 615–632. https://doi.org/10.5194/tc-15-615-2021
- Helbig, N., Schirmer, M., Magnusson, J., Mäder, F., van Herwijnen, A., Quéno, L., et al. (2021). A seasonal algorithm of the snow-covered area fraction for mountainous terrain. *The Cryosphere*, 15(9), 4607–4624. https://doi.org/10.5194/tc-15-4607-2021
- Helbig, N., van Herwijnen, A., Magnusson, J., & Jonas, T. (2015). Fractional snow-covered area parameterization over complex topography. Hydrology and Earth System Sciences, 19(3), 1339–1351. https://doi.org/10.5194/hess-19-1339-2015
- Jiang, Y., Chen, F., Gao, Y., He, C., Barlage, M., & Huang, W. (2020). Assessment of uncertainty sources in snow cover simulation in the Tibetan Plateau. *Journal of Geophysical Research: Atmospheres*, 125(18), e2020JD032674. https://doi.org/10.1029/2020JD032674
- Kang, S., Xu, Y., You, Q., Flügel, W.-A., Pepin, N., & Yao, T. (2010). Review of climate and cryospheric change in the Tibetan plateau. Environmental Research Letters, 5(1), 15101. https://doi.org/10.1088/1748-9326/5/1/015101
- Kang, Z., Qiu, B., Xiang, Z., Liu, Y., Lin, Z., & Guo, W. (2022). Improving simulations of vegetation dynamics over the Tibetan Plateau: Role of atmospheric forcing data and spatial resolution. Advances in Atmospheric Sciences, 39(7), 1115–1132. https://doi.org/10.1007/s00376-022-1426-6
- Lalande, M., Ménégoz, M., Krinner, G., Naegeli, K., & Wunderle, S. (2021). Climate change in the high mountain Asia in CMIP6. Earth System Dynamics, 12(4), 1061–1098. https://doi.org/10.5194/esd-12-1061-2021
- Lee, W.-L., Li, J.-L. F., Xu, K.-M., Suhas, E., Jiang, J. H., Wang, Y.-H., et al. (2019). Relating precipitating ice radiative effects to surface energy balance and temperature biases over the Tibetan Plateau in winter. *Journal of Geophysical Research: Atmospheres*, 124(23), 12455–12467. https://doi.org/10.1029/2018JD030204
- Lehning, M., Löwe, H., Ryser, M., & Raderschall, N. (2008). Inhomogeneous precipitation distribution and snow transport in steep terrain. Water Resources Research, 44(7), 278–284. https://doi.org/10.1029/2007WR006545
- Li, W., Guo, W., Qiu, B., Xue, Y., Hsu, P. C., & Wei, J. (2018). Influence of Tibetan Plateau snow cover on East Asian atmospheric circulation at medium-range time scales. *Nature Communications*, 9(1), 4243. https://doi.org/10.1038/s41467-018-06762-5
- Li, W., Zhang, Y., Shi, X., Zhou, W., Huang, A., Mu, M., et al. (2019). Development of land surface model BCC_AVIM2. 0 and its preliminary performance in LS3MIP/CMIP6. *Journal of Meteorological Research*, 33(5), 57–75. https://doi.org/10.1007/s13351-019-9016-y
- Liang, S., Cheng, J., Jia, K., Jiang, B., Zhou, J., Xiao, Z., et al. (2020). The Global Land Surface Satellite (GLASS) product suite. Bulletin of the American Meteorological Society, 102(2), 1–37. https://doi.org/10.1175/BAMS-D-18-0341.1
- Liang, S., Zhang, X., Xiao, Z., Cheng, J., Liu, Q., & Zhao, X. (2013). Global Land Surface Satellite (GLASS) products: Algorithms, validation and analysis (p. 171). Springer.
- Liang, S., Zhao, X., Yuan, W., Liu, S., Cheng, X., Xiao, Z., et al. (2013). A long-term Global Land Surface Satellite (GLASS) dataset for environmental studies. *International Journal of Digital Earth*, 6(sup1), 5–33. https://doi.org/10.1080/17538947.2013.805262
- Liston, G. E. (2004). Representing subgrid snow cover heterogeneities in regional and global models. *Journal of Climate*, 17(6), 1381–1397. https://doi.org/10.1175/1520-0442(2004)017<1381:RSSCHI>2.0.CO;2
- Liston, G. E., & Elder, K. (2006). A distributed snow-evolution modeling system (SnowModel). *Journal of Hydrometeorology*, 7(6), 1259–1276. https://doi.org/10.1175/JHM548.1
- Marshall, S., & Oglesby, R. J. (1994). An improved snow hydrology for GCMs. Part 1: Snow cover fraction, albedo, grain size, and age. Climate Dynamics, 10(1–2), 21–38. https://doi.org/10.1007/s003820050033
- Dynamics, 19(1–2), 21–36. https://doi.org/10.1175/1520-0442(1994)007<1251:SHIAGC>2.0.CO;2
- Meng, X., Lyu, S., Zhang, T., Zhao, L., Li, Z., Han, B., et al. (2018). Simulated cold bias being improved by using MODIS time-varying albedo in the Tibetan Plateau in WRF model. Environmental Research Letters, 13(4), 044028. https://doi.org/10.1088/1748-9326/aab44a
- Mott, R., Vionnet, V., & Grünewald, T. (2018). The seasonal snow cover dynamics: Review on wind-driven coupling processes. Frontiers of Earth Science, 6, 197. https://doi.org/10.3389/feart.2018.00197
- Niu, G., & Yang, Z. (2007). An observation-based formulation of snow cover fraction and its evaluation over large North American river basins. Journal of Geophysical Research, 112(D21), D21101. https://doi.org/10.1029/2007JD008674
- Ouyang, B., Che, T., Dai, L., & Wang, Z. (2012). Estimating mean daily surface temperature over the Tibetan Plateau based on MODIS LST products. *Journal of Glaciology and Geocryology*, 34(2), 296–303. https://doi.org/10.1007/s11783-011-0280-z
- Qin, D., Liu, S., & Li, P. (2006). Snow cover distribution, variability, and response to climate change in Western China. *Journal of Climate*, 19(9), 1820–1833. https://doi.org/10.1175/JCLI3694.1
- Roesch, A., Wild, M., & Ohmura, A. (2001). Snow cover fraction in a General Circulation Model. In *Remote sensing and climate modeling:* Synergies and limitations (pp. 203–232). https://doi.org/10.1007/0-306-48149-9_9
- Sellers, P. J., Randall, D. A., Collatz, G. J., Berry, J. A., Field, C. B., Dazlich, D. A., et al. (1996). A revised land surface parameterization (SiB2) for atmospheric GCMS. Part I: Model formulation. *Journal of Climate*, 9(4), 676–705. https://doi.org/10.1175/1520-0442(1996)009<0676: ARLSPF>2.0.CO;2
- Seol, K. H., & Hong, S. Y. (2009). Relationship between the Tibetan snow in spring and the east Asian summer monsoon in 2003: A global and regional modeling study. *Journal of Climate*, 22(8), 2095–2110. https://doi.org/10.1175/2008JCL12496.1
- Skaugen, T., & Melvold, K. (2019). Modeling the snow depth variability with a high-resolution lidar data set and nonlinear terrain dependency. Water Resources Research, 55(11), 9689–9704. https://doi.org/10.1029/2019WR025030
- Su, F., Duan, X., Chen, D., Hao, Z., & Cuo, L. (2013). Evaluation of the global climate models in the CMIP5 over the Tibetan Plateau. *Journal of Climate*, 26(10), 3187–3208. https://doi.org/10.1175/JCLI-D-12-00321.1

MIAO ET AL. 17 of 18



- Sun, S., Jin, J., & Xue, Y. (1999). A simple snow-atmosphere-soil transfer model. Journal of Geophysical Research, 104(D16), 19587–19597. https://doi.org/10.1029/1999JD900305
- Sun, S., & Xue, Y. (2001). Implementing a new snow scheme in simplified simple biosphere model. *Advances in Atmospheric Sciences*, 18(3), 335–354. https://doi.org/10.1007/BF02919314
- Swenson, S. C., & Lawrence, D. M. (2012). A new fractional snow-covered area parameterization for the Community Land Model and its effect on the surface energy balance. *Journal of Geophysical Research*, 117, D21107. https://doi.org/10.1029/2012JD018178
- Tang, Z., Wang, J., Li, H., & Yan, L. (2013). Spatiotemporal changes of snow cover over the Tibetan Plateau based on cloud-removed moderate resolution imaging spectroradiometer fractional snow cover product from 2001 to 2011. *Journal of Applied Remote Sensing*, 7(1), 2431. https://doi.org/10.1117/1.JRS.7.073582
- Usha, K. H., Nair, V. S., & Babu, S. S. (2020). Modeling of aerosol induced snow albedo feedbacks over the Himalayas and its implications on regional climate. Climate Dynamics, 54(9–10), 4191–4210. https://doi.org/10.1007/s00382-020-05222-5
- Wan, Z. (2014). New refinements and validation of the collection-6 MODIS land-surface temperature/emissivity product. Remote Sensing of Environment, 140, 36–45. https://doi.org/10.1016/j.rse.2013.08.027
- Wang, B., Ma, Y., Su, Z., Wang, Y., & Ma, W. (2020). Quantifying the evaporation amounts of 75 high-elevation large dimictic lakes on the Tibetan Plateau. Science Advances, 6(26), eaay8558. https://doi.org/10.1126/sciadv.aay8558
- Wang, J., Che, T., Li, Z., Li, H., Hao, X., Zheng, Z., et al. (2018). Investigation on snow characteristics and their distribution in China. Advances in Earth Science, 33(1), 12–15. https://doi.org/10.11867/j.issn.1001-8166.2018.01.0012
- Wang, L., Zheng, X., Sun, L., Liu, Q., & Liu, S. (2014). Validation of GLASS albedo product through Landsat TM data and ground measurements. *Journal of Remote Sensing*, 18(3), 547–558. https://doi.org/10.11834/jrs.20143130
- Wang, W., Yang, K., Zhao, L., Zheng, Z., Moore, J. C., Mamtimin, A., et al. (2020). Characterizing surface albedo of shallow fresh snow and its importance for snow ablation on the interior of the Tibetan Plateau. *Journal of Hydrometeorology*, 21(4), 815–827. https://doi.org/10.1175/ IHM.D.19.0193.1
- Wu, T., & Qian, Z. (2003). The relation between the Tibetan winter snow and the Asian summer monsoon and rainfall: An observational investigation. *Journal of Climate*, 16(12), 2038–2051. https://doi.org/10.1175/1520-0442(2003)016<2038:TRBTTW>2.0.CO;2
- Wu, T., & Wu, G. (2004). An empirical formula to compute snow cover fraction in GCMs. Advances in Atmospheric Sciences, 21(4), 529–535. https://doi.org/10.1007/BF02915720
- Xiao, C., Zhang, Y., Lofgren, B. M., & Nie, Y. (2016). The concurrent variability of East Asian subtropical and polar-front jets and its implication for the winter climate anomaly in China. *Journal of Geophysical Research: Atmospheres*, 121(12), 6787–6801. https://doi. org/10.1002/2016JD025038
- Xie, Z., Hu, Z., Xie, Z., Jia, B., Sun, G., Du, Y., & Song, H. (2018). Impact of the snow cover scheme on snow distribution and energy budget modeling over the Tibetan Plateau. *Theoretical and Applied Climatology*, 131(3–4), 951–965. https://doi.org/10.1007/s00704-016-2020-6
- Xu, Y., Shen, Y., & Wu, Z. (2013). Spatial and temporal variations of land surface temperature over the Tibetan plateau based on harmonic analysis. *Mountain Research and Development*, 33(1), 85–94. https://doi.org/10.1659/MRD-JOURNAL-D-12-00090.1
- Xue, Y., Sellers, P. J., Kinter, J. L., & Shukla, J. (1991). A simplified biosphere model for global climate studies. *Journal of Climate*, 4(3), 345–364. https://doi.org/10.1175/1520-0442(1991)004<0345:ASBMFG>2.0.CO;2
- Yan, D., Ma, N., & Zhang, Y. (2021). Development of a fine-resolution snow depth product based on the snow cover probability in the Tibetan Plateau: Validations and spatial-temporal analyses. *Journal of Hydrology*, 604, 127027. https://doi.org/10.1016/j.jhydrol.2021.127027
- Yang, K., Jie, H., Tang, W., Qin, J., & Cheng, C. (2010). On downward shortwave and longwave radiations over high altitude regions: Observation and modeling in the Tibetan Plateau. Agricultural and Forest Meteorology, 150(1), 38–46. https://doi.org/10.1016/j.agrformet.2009.08.004
- Yang, M., Zhao, W., Zhan, Q., & Xiong, D. (2021). Spatiotemporal patterns of land surface temperature change in the Tibetan plateau based on MODIS/Terra daily product from 2000 to 2018. IEEE Journal of Selected Topics in Applied Earth Observations and Remote Sensing, 14, 6501–6514. https://doi.org/10.1109/JSTARS.2021.3089851
- Yang, Z. L., Dickinson, R. E., Robock, A., & Vinnikov, K. Y. (1997). Validation of the snow submodel of the Biosphere-Atmosphere Transfer Scheme with Russian snow cover and meteorological observational data. *Journal of Climate*, 10(2), 353–373. https://doi.org/10.1175/1520-0442(1997)010<0353;VOTSSO>2.0.CO;2
- Yao, T., Wu, G., Xu, B., Wang, W., Gao, J., & An, B. (2019). Asian water tower change and its impacts. Bulletin of the Chinese Academy of Sciences, 34(11), 1203–1209. https://doi.org/10.16418/j.issn.1000-3045.2019.11.003
- Yao, T., Xue, Y., Chen, D., Chen, F., Thompson, L., Cui, P., et al. (2019). Recent Third Pole's rapid warming accompanies cryospheric melt and water cycle intensification and interactions between monsoon and environment: Multidisciplinary approach with observations, modeling, and analysis. Bulletin of the American Meteorological Society, 100(3), 423–444. https://doi.org/10.1175/BAMS-D-17-0057.1
- You, Q., Wu, T., Shen, L., Pepin, N., Aghakouchak, A., Jiang, Z., et al. (2020). Review of snow cover variation over the Tibetan plateau and its influence on the broad climate system. *Earth-Science Reviews*, 201, 103043. https://doi.org/10.1016/j.earscirev.2019.103043
- Yuan, H., Dai, Y., Xiao, Z., Ji, D., & Shangguan, W. (2011). Reprocessing the MODIS Leaf Area Index products for land surface and climate modelling. Remote Sensing of Environment, 115(5), 1171–1187. https://doi.org/10.1016/j.rse.2011.01.001
- Zhao, H., & Moore, G. W. K. (2004). On the relationship between Tibetan snow cover, the Tibetan Plateau monsoon and the Indian summer monsoon. Geophysical Research Letters, 31(14), 101–111. https://doi.org/10.1029/2004GL020040
- Zhao, P., Zhou, Z., & Liu, J. (2007). Variability of Tibetan spring snow and its associations with the hemispheric extratropical circulation and east Asian summer monsoon rainfall: An observational investigation. *Journal of Climate*, 20(15), 3942–3955. https://doi.org/10.1175/JCL14205.1
- Zhong, E., Li, Q., Sun, S., Chen, S., & Wen, C. (2017). Analysis of euphotic depth in snow with SNICAR transfer scheme: Euphotic depth in snowpack. Atmospheric Science Letters, 18(12), 484–490. https://doi.org/10.1002/asl.792
- Zhong, E., Li, Q., Sun, S., Wen, C., Chen, S., & Nath, D. (2017). Improvement of a snow albedo parameterization in the snow-atmosphere-soil transfer model: Evaluation of impacts of aerosol on seasonal snow cover. Advances in Atmospheric Sciences, 34(11), 1333–1345. https://doi.org/10.1007/s00376-017-7019-0

MIAO ET AL. 18 of 18